Airflow and Particle Deposition in a Dry Powder Inhaler: An Integrated CFD Approach

Jovana Milenkovic[1,2], Alexandros H. Alexopoulos[2], and Costas Kiparissides[1,2,3]

[1] Department of Chemical Engineering, Aristotle University of Thessaloniki,
P.O. Box 472, 54124, Thessaloniki, Greece
[2] CPERI/CERTH, 6th km Harilaou-Thermi rd., 57001, Thessaloniki, Greece
[3] Department of Chemical Engineering, The Petroleum Institute, Abu Dhabi, U.A.E.
{jovbor,aleck,cypress}@cperi.certh.gr

Abstract. An integrated computational model of a commercial Dry Powder Inhaler, DPI, device (i.e., Turbuhaler) is developed. The steady-state flow in a DPI is determined by solving the Navier-Stokes equations using FLUENT (v6.3) considering different flow models, e.g., laminar, k-ε, k-ω SST. Particle motion and deposition are described using an Eulerian-fluid/Lagrangian-particle approach. Particle/wall collisions are taken to result in deposition when the normal collision velocity is less than a size-dependent critical value. The flow rate and particle deposition are determined for a range of pressure drops (i.e., 800-8800Pa), as well as particle sizes corresponding to single particles and aggregates (i.e., 0.5-20μm). Overall, the simulation results are found to agree well with available experimental data for the volumetric outflow rate as well as the local and total particle deposition.

Keywords: Dry Powder Inhaler, Turbuhaler, CFD, Particle, Deposition.

1   Introduction

Dry Powder Inhalers, DPI, are one of the principle means of delivering pharmaceuticals due to their ease of use and cost-effectiveness [16]. The main function of a DPI device is the adequate dispersion and delivery of particles. Initially particles are in the form of a loose powder which, under the action of airflow, is broken up and dispersed as particle aggregates, which are then further broken up into fine particles [4, 18, 20, 15, 3]. Powder properties, e.g., cohesion, charge, size, and size distribution, influence powder dispersion and the breakage of particle aggregates [13, 24, 12, 7].

One of the common problems with DPIs is the loss of powder/drug due to deposition within the device. In order to provide the maximum drug dose per inhalation and to ensure minimal dose-to-dose variation it is necessary to minimize drug losses due to internal deposition. Moreover, it is desired to have good control over the dispersibility of the powder, release of drug (when attached to powder particles), and breakup of aggregates in order to achieve the desired particle/aggregate size distributions at the DPI mouthpiece outflow [3]. Consequently, if the underlying

processes are better understood one can achieve the desired outflow particle distribution which will conceivably minimize oropharyngeal losses and also permit better targeting for drug delivery in the respiratory tract.

Due to the complex and transient flow structures as well as the dynamic powder breakup and dispersion processes observed in most commercial DPIs only a small number of Computational Fluid Dynamics, CFD, investigations have been conducted [19, 17, 16]. Systematic computational studies have led to a better understanding of the function of DPI devices. For example, Coates et al. [8, 9, 10] studied the Aerolizer DPI in detail including the effects of air-intake, mouthpiece, and internal grid which led to improvements in the design and function of the DPI. Recently, the discrete element method, DEM, coupled to continuous phase-models has been implemented to describe the powder dispersion process within the inhaler [21, 6]. From the current state-of-the-art it is clear that the proper description of the aggregate strength as well as the particle/aggregate interaction with the inhaler walls are key processes that determine the final dispersion and size distribution of pharmaceutical powders [2].

The Turbuhaler (AstraZeneca) is a multidose DPI widely used to deliver a number of drugs (typically for asthma), e.g., terbutaline sulphate, (as Bricanyl), or budesonide (as Pulmicort), to the upper respiratory tract [23]. Each dose is initially in the form of loosely packed particle aggregates, ~1-20μm in size, which are released into a mixing/dispersion chamber, where they are partially broken up into particles which are then directed to the inhalation channel of the device [22, 23]. The proper function of the Turbuhaler is dependent on the dynamic volumetric flow as well as the peak inspiratory flow rate, PIFR, attained during inhalation, the amount of particles lost due to deposition within the device, and the adequate dispersion and breakup of the powder aggregates in the airflow exiting the mouthpiece. Recent experimental investigations have provided detailed information on particle deposition as well as the fine particle fraction and particle size distribution, PSD, of escaped particles in the outlet flow [11, 14, 1].

In this work the steady airflow in a Turbuhaler DPI is determined by CFD simulations and particle motion as well as deposition is determined by Eulerian-Fluid/Lagrangian-Particle, EFLP, simulations. In what follows the DPI geometry, the discretization procedure, and the CFD simulations are described in detail. Next the results for steady-state airflow are presented follow by the results for particle deposition. Finally, the computational results are compared to available experimental data.

2   Integrated Computational Model

The computational modeling of a DPI device is a challenging problem involving airflow, powder dispersion, aggregate breakup, and particle deposition. These are different processes operating at different spatial and temporal scales which require specific computational treatments (Figure 1). Fluid flow is typically described by CFD and can be treated separately from particle motion for small particle volume fractions (i.e., <10%). For larger volume fractions other approaches, e.g., two-phase or granular flow models, are necessary. Recently the DEM has been utilized to track the motions and interactions of individual particles in aggregates during the initial
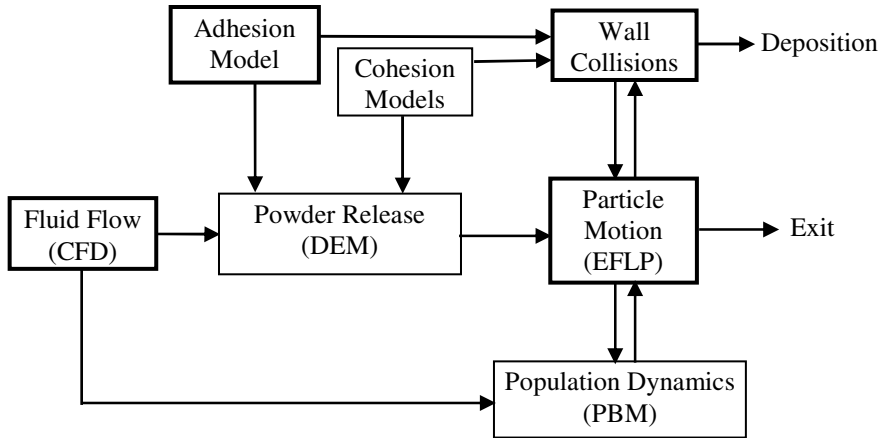
Fig. 1. Integrated computational model of a DPI. Limiting case indicated by bold boxes.

powder dispersion [6]. Particle-particle cohesion forces dominate the initial powder release and breakage of particle aggregates. The EFLP approach can be employed to follow the motion of individual particles and aggregates in the DPI. Collisions of particles with the DPI walls occur predominantly due to inertial impaction. The particle-wall collision frequency and capture efficiency (controlled by adhesion forces) determine the rate of deposition while particle cohesion forces control the rate of collision-induced breakage. Finally, the population dynamics of aggregates/ particles can be described by population balance models, PBM, if the controlling driving functions (e.g., breakage, aggregation, deposition and redispersion) can be described.

This work focuses on the limiting case of weak cohesion forces and rapid powder dispersion. In this case the powder is assumed to instantaneously break-up into a population of particles and aggregates identical to that of the free-flowing powder after which no more breakage or aggregation occurs. Consequently, the model consists of a CFD module, an EFLP module, a collision model, and an adhesion-controlled capture–efficiency model (Figure 1). Although this approach represents a limiting case it provides a means for evaluating the effects of flow rate, particle size, and adhesion forces on the local and total particle deposition in the DPI device.

The CFD approach consists of solving the continuity and momentum equations in each cell of a discretized computational domain that represents the air passage in the Turbuhaler DPI. The mass and momentum conservation equations can be expressed in scalar form as

$$\frac{\partial \rho \varphi}{\partial t} + \nabla \cdot (\rho \varphi \mathbf{u}) = \nabla \cdot \Gamma \nabla \varphi + S_{\varphi} \tag{1}$$

where ϕ is a scalar quantity (e.g., velocity component, temperature, concentration), Γ is the diffusivity coefficient, and S_{ϕ} is the source term.

Particle pathlines can be determined by the EFLP approach, that is, by solving the following force balance equation for each particle assuming an unperturbed airflow solution.

$$\frac{du_p}{dt} = F_D\left(u - u_p\right) + g\left(1 - \rho/\rho_p\right) + F_B + F \tag{2}$$

where the terms on the right hand side represent the drag force per unit particle mass, the gravitational acceleration per unit mass, the Brownian forces, and additional acceleration terms (e.g., Saffman lift force).

When particle trajectories intercept the DPI walls a particle-wall collision takes place which can result in deposition or particle rebound. In this work the capture efficiency, σ, is related to the normal particle collision velocity, v_n, according to

$$\sigma = 1 - H(v_n / v_c) \tag{3}$$

where H is the Heaviside function and v_c is the critical collision velocity which, according to the developments of Brach and Dunn [5], is given by:

$$v_c = \left(\frac{2E}{D}\right)^{10/7} \tag{4}$$

where D is the particle diameter and the effective stiffness parameter E is given by

$$E = 0.51\left(\frac{5\pi^2\left(k_s + k_p\right)}{4\rho^{3/2}}\right)^{2/5} \tag{5}$$

and k_s and k_p are determined by:

$$k_s = \frac{1 - v_s^2}{\pi E_s} \text{ and } k_p = \frac{1 - v_p^2}{\pi E_p} \tag{6}$$

where v_s and v_p and E_s and E_p are the Poisson's ratio and Young's modulus of the surface and particle, respectively. In the case of lactose particles ($v_p = 0.4$, $E_p = 1.0$GPa) colliding with polystyrene surfaces ($v_s = 0.35$, $E_s = 4.1$GPa) the critical velocity was determined to be $v_c = 2.7$m/s.

3   Results

The Turbuhaler DPI geometry was constructed in a CAD/CAM environment (i.e., CATIA v5 R19) and then imported into GAMBIT (v2.1) where the airflow domain was defined and a series of computational grids were constructed consisting of 2×10^5 – 2×10^6 tetrahedral cells with a maximum skewness of 0.85 (Figure 2). The computational grids were originally refined in regions where large gradients of flow were expected. Further refinements were conducted within FLUENT based on actual velocity gradients observed in initial solutions. It should be noted that the computational domain was extended from the mouthpiece outlet by 20mm in order to minimize recirculation effects at the outflow surface and to improve convergence behavior.

The Navier-Stokes equations for flow were solved using the commercial CFD software (i.e., FLUENT v6.3). The SIMPLEC scheme was employed to describe pressure-velocity coupling. Second order discretization was used for pressure and third order MUSCL for momentum and turbulent variables. Convergence of CFD simulations was assumed when the residuals were $< 10^{-4}$. Zero gauge pressure boundary conditions were employed at all the inflows, i.e., two powder loaded cylinders (see bottom of Figure 2) and four extra air inlets in the DPI circulation
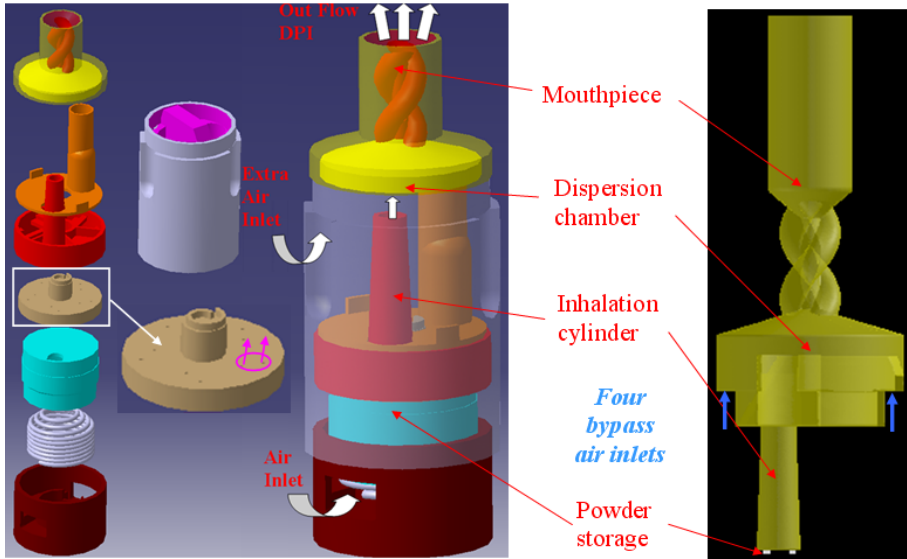
Fig. 2. Turbuhaler Dry Powder Inhaler CAD model and Computational Grid

chamber. Different steady state airflows (i.e., 20 to 70 l/min) were simulated by imposing a wide range of pressure drops at the mouthpiece outflow ranging from 800 to 8800Pa.

EFLP simulations of particle motion and deposition were conducted for particles between 0.5-20μm in size encompassing the range of single particle and particle aggregate sizes of typical pharmaceutical powders employed in the Turbuhaler DPI. Particles were assumed to be released instantaneously at t = 0 and uniformly from circular surfaces located immediately upstream (i.e., 2mm) from the powder storage sites. Powder dispersion was assumed to occur instantaneously after which no further breakage occurred. This assumption corresponds to the limit of very weak particle cohesion forces. After the initial powder release and aggregate breakage, particles in motion were taken to be constant in size.

3.1 Simulations of Airflow in the Turbuhaler DPI

According to the range of volumetric airflows examined in this work, e.g. Q = 20 – 70 l/min, the local Reynolds numbers, Re = Q ρ / μ A$^{1/2}$, where ρ and μ are the density and the viscosity of air and A is the cross-sectional area, ranged from 130-16,000.

Consequently the transitional SST k-ω model was employed to describe the turbulent flows encountered in the DPI. Grid convergence was verified for the SST k-ω model with the 1 10^6 grid providing essentially identical results as the 2 10^6 grid and was used for the results presented in this paper.

In Figure 3 the velocity magnitudes as well as the tangential and radial velocities are displayed along an axial (i.e., zx) plane. As can be observed, the airflow in the DPI device is found to be laminar in the inhalation channel with two jet flows
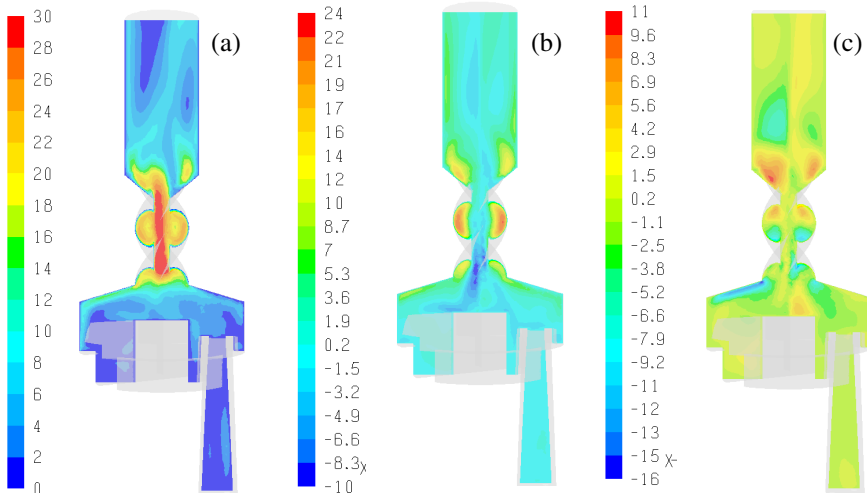
Fig. 3. Velocity contours in the Turbuhaler DPI: k-ω SST (ΔP = 800Pa). (a) velocity magntude, (b) tangential velocity, (c) radial velocity

Fig. 4. Velocity contours in the Turbuhaler DPI: LES (ΔP = 800Pa). (a) velocity magnitude, (b) tangential velocity, (c) radial velocity

emanating from the powder storage cylinders. In the circulation chamber the flow is characterized by large eddies and secondary flows. In the helical region significant tangential flows develop (reaching 83% of the maximum velocity magnitude) and persist about halfway up the mouthpiece extension. It should be noted that the velocity profiles observed for larger flow rates, e.g., 60 l/min, are qualitatively similar.

Large Eddy Simulations, LES, fully resolve the large scale motion of turbulent flows thus providing more information and accurate results compared to Reynolds Averaged Navier-Stokes, RANS, approaches, e.g., k-ε, k-ω. The computational burden of LES is significant (e.g., at least an order of magnitude more than with RANS models). Consequently, only a single case (i.e., ΔP = 800Pa) of steady-state flow in the Turbuhaler DPI was simulated with LES using FLUENT. In Figure 4 the results for the mean velocity magnitude, as well as the radial and tangential components obtained with LES are shown. The main flow structures are similar with the k-ω SST results in Figure 3 but differences can be observed in the details of the flow, e.g., the secondary flows in the mouthpiece extension. The intensity of fluctuations (e.g., RMS velocity / velocity magnitude) varied within the device up to a value of ~50% indicating significant local fluctuations around the mean for the length scales resolved within the LES. The RMS range from 1-8m/s for the axial velocity component and 1-4m/s for the other components with different spatial variations within the device.
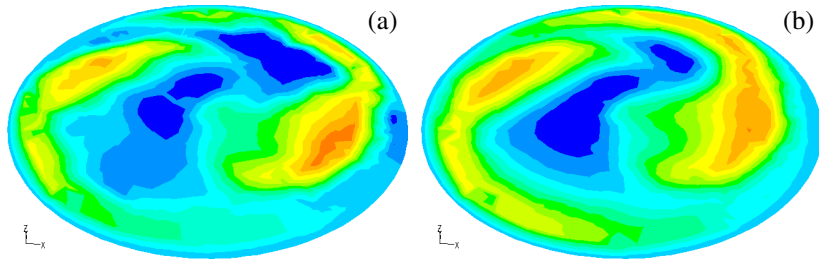

Fig. 5. Tangential velocity component at the mouthpiece exit (ΔP = 1400Pa).(a) LES (b) k-ω SST

In Figure 5 the tangential velocities at the outlet surface for ΔP = 1400Pa are shown. It is clear that the tangential velocities predicted by the k-ω SST and LES turbulence models are very similar. In fact the k-ω SST turbulence model provided the most similar to the LES results compared to the other RANS turbulence models (e.g., standard k-ε, RNG k-ε). Consequently, despite the observed differences in secondary flows, the k-ω SST model was employed for all the simulations of this work.

3.2   Simulation of Particle Motion and Deposition in the Turbuhaler DPI

Particle simulations were performed for all the flows examined in section 3.1. For effective powder dispersion the solids volume ratio in the DPI device is approximately 10^{-2}-10^{-4} depending on the location and the flow rate. Consequently,

the particle phase will not influence the airflow solution and the EPLF approach can be employed. A wide range of injected particle numbers was used (i.e., 2,000-40,000). It was found that a minimum of 5,000 particles were necessary to obtain number-independent deposition results. The capture efficiency was implemented internally within FLUENT using a user-defined function.

   Simulations with injections of single-sized particles as well as with particle size distributions ranging from 0.5-20μm were performed. The spatial distribution of particles deposited on the DPI walls was visualized using Tecplot. In Figure 6 the effect of particle size on the distribution of deposited particles in the DPI device is shown. Comparing particle sizes of 1, 2 and 5μm significant differences in the total
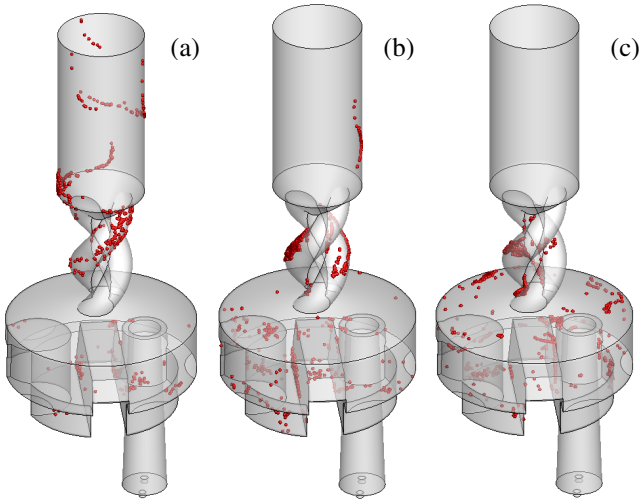

Fig. 6. Particle Deposition – Effect of Particle Size. $\Delta P = 800$Pa, $\sigma = 1$, (a), D = 1μm, (b) D = 2μm, (c) D = 5μm.

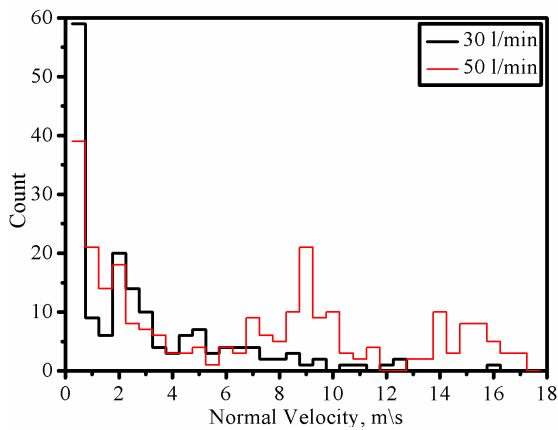**Fig. 7.** Distribution of normal collision velocities ($\sigma = 1$, D = 2μm, $\Delta P = 1400$Pa)

deposition as well as the deposition distribution are observed. The significant particle deposition that occurs in the mouthpiece region (including the helical region) is actually a common problem in many commercial DPI devices where about half the internal deposition occurs [11].

The distribution of particle collision characteristics, i.e., normal velocities and collision angles were examined for two volumetric flow rates (i.e., Q = 30 and 50 l/min). In Figure 7 the distributions of normal collision velocities are shown. For small flow rates (i.e., Q = 30 l/min) most of the particle collisions occur with normal velocities v_n < 1 m/s. resulting in particle capture. At larger flow rates (i.e., Q = 50 l/min) the number of particle collisions increases and shifts to larger values of normal velocity with a significant proportion between 8-10 m/s which result in rebound. It should be noted that most of the particle collisions occurred with a collision angle between 5-10° and 10-18° for Q = 30 and 50 l/min, respectively.
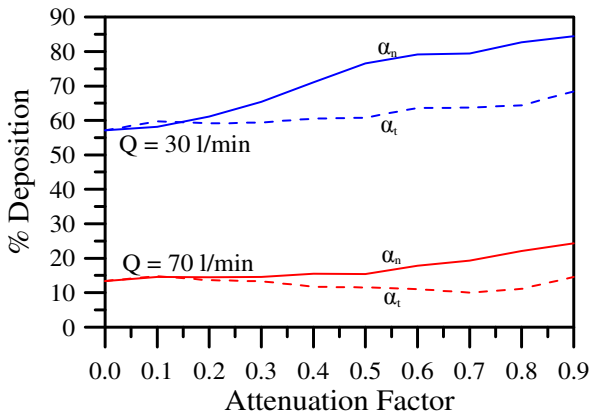

Fig. 8. Effect of attenuation factors (D = 2μm, ΔP = 1400Pa)
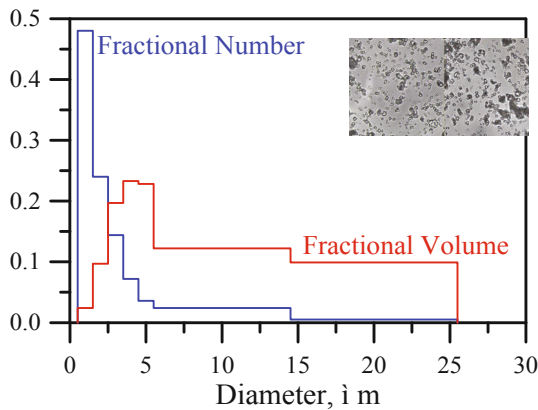

Fig. 9. Fractional particle number and volume distribution

The effect of momentum loss of rebounding particles after collision with the DPI walls was also examined. In Figure 8 the effect of a wide range of normal and tangential attenuations factors, α_n and α_t, on the total deposition of 2μm particles for Q = 30 and 70 l/min is shown. It is clear that attenuation has a more significant effect on the total deposition for the low volumetric flow case (i.e., Q = 30 l/min). Furthermore, particle deposition is more sensitive to normal attenuation than the corresponding tangential term.

Figure 9 displays the PSD of freely flowing powder containing Budesonide (Pulmicort). The peak in the number distribution is at D_0 = 2.2μm while for the volume distribution it is at 4.5μm. It was found that a Rosin-Rammler distribution, f(D), with a shape parameter value of n = 1 and a mean diameter of D_0 = 2.2μm, i.e., is a good approximation to the distribution depicted in Figure 9.

$$f(D) = (1/D_0)\, e^{-D/D_0} \tag{7}$$

The injected, escaped and deposited fractional volume distributions for ΔP= 800Pa are provided in Figure 10. It is observed that, there are very large differences in both the amounts and size distributions of escaped and deposited particles depending on the value of the capture efficiency, i.e., σ = 1 or σ evaluated by eqs. 3-6. It should be noted that small particles (e.g., 1-5μm) exhibit fewer collisions but have a larger capture efficiency than large particles (e.g., 5-10μm).

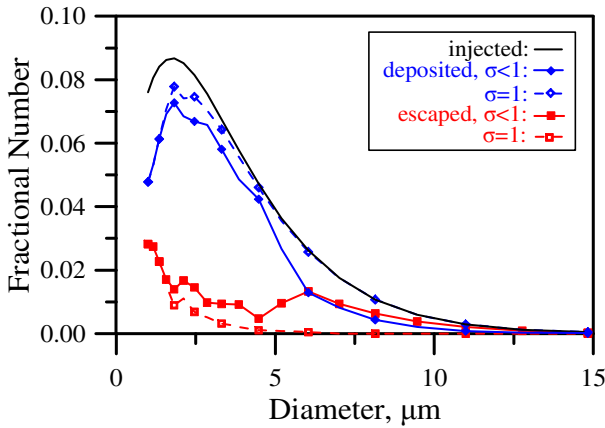**Fig. 10.** Particle Deposition. (a) Fractional Cumulative Deposition, (b) Local.Deposition (ΔP = 800Pa).

3.3   Comparison to Experimental Data

The computational results of this work were compared to the experimental results of de Koning et al [11] and Abdelrahim [1] for the Turbuhaler in terms of flow and particle deposition. In Figure 11 the predicted steady-state volumetric flows are plotted against

the outlet pressure drop applied at the mouthpiece. Both laminar and k-ω SST models for flow are examined. It is clear that both models agree very well with the experimental data for all flow rates with the k-ω SST model being slightly more accurate.

In Figure 12 the total, circulation chamber, and mouthpiece particle depositions for 1400Pa (corresponding to Q = 30 l/min) are compared to the experimental data of de Koning et al. [11]. The mouthpiece, circulation chamber, and total particle deposition results for Q = 30 l/min are in good agreement to the experimental data.

In Figure 13 the predicted total particle deposition are compared to the experimental data of de Koning et al [11] and Abdelrahim [1] for flowrates Q = 30, 40, 50, 60 and 70 l/min and for two different inspired volumes, i.e., 2 and 4l [1].
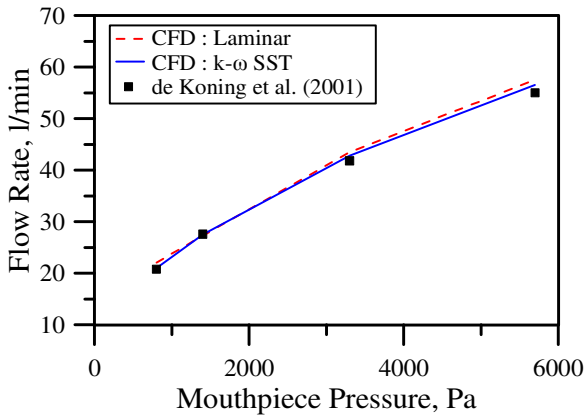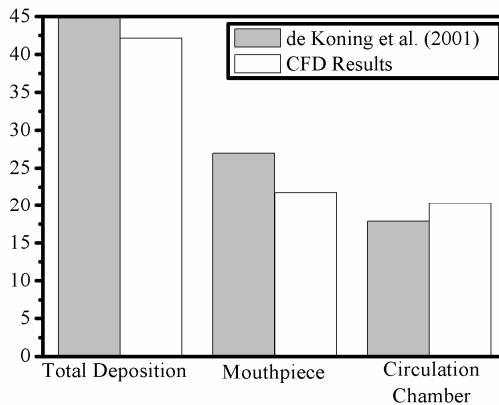

Fig. 11. Volumetric flow in the Turbuhaler

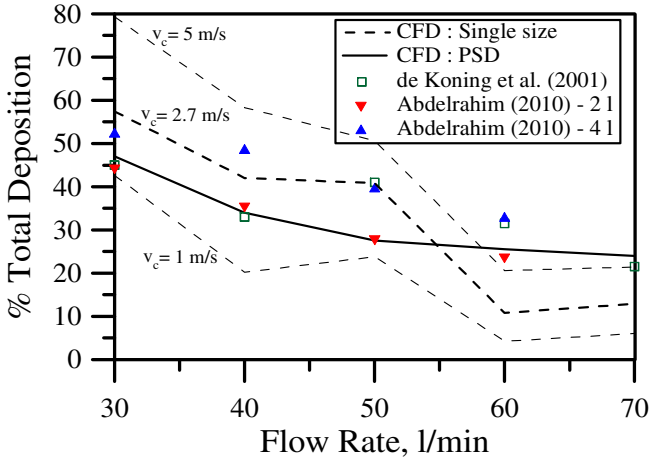**Fig. 12.** Regional particle deposition in the Turbuhaler. Q = 30 l/min.

Fig. 13. Total particle deposition in the Turbuhaler. D = 2 μm. V_c = 2.7 m/s. Comparison between experimental results of de Koning et al. [11], Abdelrahim [1] and computational CFD results.

Simulations with injections of particles following a PSD characterized by eq. (6) were performed. The computational results were found to agree well with the experimental data. Simulations with injections of single-sized particles were also performed. For a particle diameter of D = 2μm and a critical velocity of v_c = 2.7m/s the agreement with the experimental data is good considering the different experimental conditions (e.g., dynamic inhalation vs. steady state simulations) and the model simplifications and assumptions. Different values of v_c are also shown in Figure 13 to provide an indication of the sensitivity of the computed particle deposition on the value of v_c.

4   Conclusions

This work has demonstrated the use of CFD to determine the complicated airflow as well as particle motion and deposition in the Turbuhaler DPI. As the flow was either locally laminar or transitionally turbulent the transitional SST k-ω model for turbulence was employed. The simulations revealed complicated flows with intense recirculation patterns in the circulation chamber and strong tangential flows in the helical region of the mouthpiece. LES results revealed some differences in the large eddies and secondary flows but were otherwise closest to the k-ω SST results. LES results also indicated that the fundamental assumption of local turbulence isotropy of the RANS models is incorrect and requires further investigation.

   Particle deposition was found to depend on size and flow rate and occurred predominantly in the circulation chamber and the mouthpiece. The computational solutions were compared to experimental data for volumetric flow and regional deposition of de Koning et al. [11] and good agreement was observed. A simple collision model by Brach and Dunn [5] was employed to determine the critical velocity for particle capture, i.e., v_c, which was found to produce total particle depositions similar to the experimental values of de Koning et al [11] and Abdelrahim [1].

Future work will involve the simulation of dynamic inhalations, collision-induced breakage and will elaborate on the particle collision model which can be extended by including the effects of particle properties (e.g., size, shape, and charge), surface properties (e.g., roughness, charge), as well as humidity.

References

1. Abdelrahim, M.E.: Emitted dose and lung deposition of inhaled terbutaline from Turbuhaler at different conditions. Respiratory Medicine 104, 682–689 (2010)
2. Adi, S., Adi, H., Chan, H.-K., Finlay, W.H., Tong, Z., Yang, R., Yu, A.: Agglomerate strength and dispersion of pharmaceutical powders. J. Aerosol Science. 42, 285–294 (2011)
3. Alagusundaram, M., Deepthi, N., Ramkanth, S., Angalaparameswari, S., Saleem, T.S.M., Gnanaprakash, K., Thiruvengadarajan, V.S., Madhusudhana, C., Alagusundaram, C.M., et al.: Dry Powder Inhalers - An Overview. Int. J. Res. Pharm. Sci. 1(1), 34–42 (2010)
4. Ashurst, I., Malton, A., Prime, D., Sumby, B.: Latest advances in the development of dry powder inhalers. PSTT 3(7), 246–256 (2000)
5. Brach, R.M., Dunn, P.F.: A Mathematical Model of Impact and Adhesion of Microspheres. Aerosol Sci. Technol. 23, 51–71 (1992)
6. Calvert, G., Hassanpour, A., Ghadiri, M.: Mechanistic analysis and computer simulation of the aerodynamic dispersion of loose aggregates. Chemical Engineering Research and Design 89, 519–525 (2011)
7. Chan, H.-K.: Dry powder aerosol drug delivery – Opportunities for colloid and surface scientists, Colloids and Surfaces A: Physicochem. Eng. Aspects 284-285, 50–55 (2006)
8. Coates, M.S., Fletcher, D.F., Chan, H.-K., Raper, J.A.: Effect of Design on the Performance of a Dry Powder Inhaler Using Computational Fluid Dynamics. Part 1: Grid Structure and Mouthpiece Length. J. of Pharmaceutical Sciences 93, 2863–2876 (2004)
9. Coates, M.S., Chan, H.-K., Fletcher, D.F., Raper, J.A.: Influence of Air Flow on the Performance of a Dry Powder Inhaler Using Computational and Experimental Analyses. Pharmaceutical Research 22(9), 923–932 (2005)
10. Coates, M.S., Chan, H.-K., Fletcher, D.F., Raper, J.A.: Effect of Design on the Performance of a Dry Powder Inhaler Using Computational Fluid Dynamics. Part 2: Air Inlet Size. J. of Pharmaceutical Sciences 95(6), 1382–1392 (2006)
11. de Koning, J.P., Visser, M.R., Oelen, G.A., de Boer, A.H., van der Mark, T.W., Coenegracht, P.M.J., Tromp, T.F.J., Frijlink, H.W.: Effect of Peak Inspiratory Flow and Flow Increase Rate on In Vitro Drug Deposition from Four Dry Powder Inhaler Devices. In: Dry Powder Inhalation: Technical and Physiological Aspects, Prescribing and Use, Thesis, Rijksuniversiteit Groningen, ch. 6, pp. 83–94 (2001)
12. Finlay, W.: The Mechanics of Inhaled Pharmaceutical Aerosols. An Introduction. Academic Press, London (2001)
13. French, D.L., Edwards, D.A., Niven, R.W.: The Influence of Formulation on Emission Deaggregation and Deposition of Dry Powders for Inhalation. J. Aerosol Sci. 27(5), 769–783 (1996)

14. Hoe, S., Traini, D., Chan, H.-K., Young, P.M.: Measuring charge and mass distributions in dry powder inhalers using the electrical Next Generation Impactor (eNGI). European J. of Pharmaceutical Science 38, 88–94 (2009)
15. Islam, N., Gladki, E.: Dry powder inhalers (DPIs) - A review of device reliability and innovation. Int. J. of Pharmaceutics 360, 1–11 (2008)
16. Islam, N., Clearly, M.J.: Developing an efficient and reliable dry powder inhaler for pulmonary drug delivery – A review for multidisciplinary researchers. Medical Engineering & Physics 34, 409–427 (2012)
17. Ligotke, M.W.: Development and characterization of a dry powder inhaler. In: Dalby, R.N., Byron, P.R., Peart, J., Farr, S.J. (eds.) Respiratory Drug Delivery VIII, vol. I, pp. 419–422. Serentec Press Inc., Tucson (2002)
18. Newman, S.P., Busse, W.W.: Evolution of dry powder inhaler design, formulation, and performance. Respir. Med. 96(5), 293–304 (2002)
19. Schuler, C., Bakshi, A., Tuttle, D., Smith, A., Paboojian, S., Snyder, H., Rasmussen, D., Clark, A.: Inhale's dry-powder pulmonary drug delivery system: Challenges to current modeling of gas-solid flows. In: Proceedings of FEDSM 1999: 3rd ASME/JSME Joint Fluids Engineering Conference and 1999 ASME Fluids Engineering Summer Meeting, FEDSM 1999-7895 (1999)
20. Tobyn, M., Staniforth, J.N., Morton, D., Harmer, Q., Newton, M.E.: Active and intelligent inhaler device development. Int. J. of Pharmaceutics 277, 31–37 (2004)
21. Tong, Z.B., Yang, R.Y., Chu, K.W., Yu, A.B., Adi, S., Chan, H.-K.: Numerical study of the effects of particle size and polydispersity on the agglomerate dispersion in a cyclonic flow. Chemical Engineering Journal 164, 432–441 (2010)
22. Tsima, M.P., Martin, G.P., Marriott, C., Gardenton, D., Yianneskis, M.: Drug delivery to the respiratory tract using dry powder inhaler. Int. J. of Pharmaceutics 101, 1–13 (1994)
23. Wetterlin, K.: Turbuhaler: A New Powder Inhaler for Administration of Drugs to the Airways. Pharmaceutical Research 5(8), 506–508 (1988)
24. Zeng, X.-M., Martin, G.P., Marriott, C., Pritchard, J.: The influence of carrier morphology on drug delivery by dry powder inhalers. Int. J. of Pharmaceutics 200, 93–106 (2000)